Research Article | Vol. 25, No. 24 | 27 Nov 2017 | OPTICS EXPRESS 29560
Optics EXPRESS

Numerical investigation of a scalable setup for efficient terahertz generation using a segmented tilted-pulse-front excitation

LÁSZLÓ PÁLFALVI,[1,*] GYÖRGY TÓTH,[2] LEVENTE TOKODI,[1] ZSUZSANNA MÁRTON,[1] JÓZSEF ANDRÁS FÜLÖP,[2,3] GÁBOR ALMÁSI,[1,3] AND JÁNOS HEBLING[1,2,3]

[1]*Institute of Physics, University of Pécs, Ifjúság ú. 6, 7624 Pécs, Hungary*
[2]*MTA-PTE High-Field Terahertz Research Group, Ifjúság ú. 6, 7624 Pécs, Hungary*
[3]*Szentágothai Research Centre, University of Pécs, Ifjúság ú. 20, 7624 Pécs, Hungary*
**palfalvi@fizika.ttk.pte.hu*

Abstract: A hybrid-type terahertz pulse source is proposed for high energy terahertz pulse generation. It is the combination of the conventional tilted-pulse-front setup and a transmission stair-step echelon-faced nonlinear crystal with a period falling in the hundred-micrometer range. The most important advantage of the setup is the possibility of using plane parallel nonlinear optical crystal for producing good-quality, symmetric terahertz beam. Another advantage of the proposed setup is the significant reduction of imaging errors, which is important in the case of wide pump beams that are used in high energy experiments. A one dimensional model was developed for determining the terahertz generation efficiency, and it was used for quantitative comparison between the proposed new hybrid setup and previously introduced terahertz sources. With lithium niobate nonlinear material, calculations predict an approximately ten-fold increase in the efficiency of the presently described hybrid terahertz pulse source with respect to that of the earlier proposed setup, which utilizes a reflective stair-step echelon and a prism shaped nonlinear optical crystal. By using pump pulses of 50 mJ pulse energy, 500 fs pulse length and 8 mm beam spot radius, approximately 1% conversion efficiency and 0.5 mJ terahertz pulse energy can be reached with the newly proposed setup.

© 2017 Optical Society of America

OCIS codes: (190.7110) Ultrafast nonlinear optics; (260.3090) Infrared, far; (300.6495) Spectroscopy, terahertz.

References and links

1. A. Fallahi, M. Fakhari, A. Yahaghi, M. Arrieta, and F. X. Kärtner, "Short electron bunch generation using single-cycle ultrafast electron guns," Phys. Rev. Accel. Beams **19**(8), 081302 (2016).
2. E. A. Nanni, W. R. Huang, K.-H. Hong, K. Ravi, A. Fallahi, G. Moriena, R. J. Miller, and F. X. Kärtner, "Terahertz-driven linear electron acceleration," Nat. Commun. **6**, 8486 (2015).
3. Z. Tibai, L. Pálfalvi, J. A. Fülöp, G. Almási, and J. Hebling, "THz-pulse-driven particle accelerators," in *4th EOS Topical Meeting on Terahertz Science & Technology* (Italy, 2014).
4. L. Pálfalvi, J. A. Fülöp, G. Tóth, and J. Hebling, "Evanescent-wave proton postaccelerator driven by intense THz pulse," Phys. Rev. Spec. Top. Accel. Beams **17**(3), 031301 (2014).
5. A. Sharma, Z. Tibai, and J. Hebling, "Intense tera-hertz laser driven proton acceleration in plasmas," Phys. Plasmas **23**(6), 063111 (2016).
6. J. Hebling, G. Almási, I. Kozma, and J. Kuhl, "Velocity matching by pulse front tilting for large area THz-pulse generation," Opt. Express **10**(21), 1161–1166 (2002).
7. Q. Wu and X. C. Zhang, "Ultrafast electro-optic field sensors," Appl. Phys. Lett. **68**(12), 1604–1606 (1996).
8. J. Hebling, A. G. Stepanov, G. Almási, B. Bartal, and J. Kuhl, "Tunable THz pulse generation by optical rectification of ultrashort laser pulses with tilted pulse fronts," Appl. Phys. B **78**, 593–599 (2004).
9. J. A. Fülöp, Z. Ollmann, C. Lombosi, C. Skrobol, S. Klingebiel, L. Pálfalvi, F. Krausz, S. Karsch, and J. Hebling, "Efficient generation of THz pulses with 0.4 mJ energy," Opt. Express **22**(17), 20155–20163 (2014).
10. L. Tokodi, A. Buzády, J. Hebling, and L. Pálfalvi, "Possibility of high-energy THz generation in $LiTaO_3$," Appl. Phys. B **122**(9), 235 (2016).
11. J. A. Fülöp, G. Polónyi, B. Monoszlai, G. Andriukaitis, T. Balciunas, A. Pugzlys, G. Arthur, A. Baltuska, and J. Hebling, "Highly efficient scalable monolithic semiconductor terahertz pulse source," Optica **3**(10), 1075–1078 (2016).

#302512 https://doi.org/10.1364/OE.25.029560
Journal © 2017 Received 17 Jul 2017; revised 19 Sep 2017; accepted 22 Sep 2017; published 13 Nov 2017

Optics EXPRESS

12. G. Polónyi, M. I. Mechler, J. Hebling, and J. A. Fülöp, "Prospects of Semiconductor Terahertz Pulse Sources," IEEE J. Sel. Top. Quantum Electron. **23**(4), 1–8 (2017).
13. L. Pálfalvi, J. A. Fülöp, G. Almási, and J. Hebling, "Novel setups for extremely high power single-cycle terahertz pulse generation by optical rectification," Appl. Phys. Lett. **92**(17), 171107 (2008).
14. J. A. Fülöp, L. Pálfalvi, G. Almási, and J. Hebling, "Design of high-energy terahertz sources based on optical rectification," Opt. Express **18**(12), 12311–12327 (2010).
15. Z. Ollmann, J. Hebling, and G. Almási, "Design of a contact grating setup for mJ-energy THz pulse generation by optical rectification," Appl. Phys. B **108**(4), 821–826 (2012).
16. M. Tsubouchi, K. Nagashima, F. Yoshida, Y. Ochi, and M. Maruyama, "Contact grating device with Fabry-Perot resonator for effective terahertz light generation," Opt. Lett. **39**(18), 5439–5442 (2014).
17. L. Pálfalvi, Z. Ollmann, L. Tokodi, and J. Hebling, "Hybrid tilted-pulse-front excitation scheme for efficient generation of high-energy terahertz pulses," Opt. Express **24**(8), 8156–8169 (2016).
18. B. K. Ofori-Okai, P. Sivarajah, W. Ronny Huang, and K. A. Nelson, "THz generation using a reflective stair-step echelon," Opt. Express **24**(5), 5057–5068 (2016).
19. K. L. Vodopyanov, "Optical generation of narrow-band terahertz packets in periodically inverted electro-optic crystals: conversion efficiency and optimal laser pulse format," Opt. Express **14**(6), 2263–2276 (2006).
20. J. A. Fülöp, L. Pálfalvi, G. Almási, and J. Hebling, "Design of high-energy terahertz sources based on optical rectification: erratum," Opt. Express **19**(23), 22950 (2011).
21. J. Hebling, "Derivation of the pulse front tilt caused by angular dispersion," Opt. Quantum Electron. **28**(12), 1759–1763 (1996).
22. M. I. Bakunov and S. B. Bodrov, "Terahertz generation with tilted-front laser pulses in a contact-grating scheme," J. Opt. Soc. Am. B **31**(11), 2549–2557 (2014).
23. L. Pálfalvi, J. Hebling, J. Kuhl, A. Peter, and K. Polgar, "Temperature dependence of the absorption and refraction of Mg-doped congruent and stoichiometric $LiNbO_3$ in the THz range," J. Appl. Phys. **97**(12), 123505 (2005).
24. C. Lombosi, G. Polónyi, M. Mechler, Z. Ollmann, J. Hebling, and J. A. Fülöp, "Nonlinear distortion of intense THz beams," New J. Phys. **17**(8), 083041 (2015).
25. K. Ravi, W. R. Huang, S. Carbajo, X. Wu, and F. Kärtner, "Limitations to THz generation by optical rectification using tilted pulse fronts," Opt. Express **22**(17), 20239–20251 (2014).

1. Introduction

Acceleration of electrons [1–3] and protons [4, 5] are new, promising applications of intense THz pulses. Optical rectification of ultrashort laser pulses in nonlinear materials (NM) is a standard way for efficient THz generation. Since the introduction of the tilted-pulse-front technique [6], the velocity matching has become possible also in those cases, where good nonlinear optical properties of the material are vitiated by the large difference between the optical and the terahertz refractive indices. Presently, this standard, efficient method is applied for various materials. Lithium niobate (LN), having extremely high (168 pm/V [7, 8]) effective nonlinear optical coefficient and terahertz refractive index approximately twice as large as the optical refractive index, is one of the most important materials [9] at around 1 μm pump wavelength. Lithium tantalate (LT), having similarly good optical properties, is a good alternative at shorter (800 nm) pump wavelengths [10], where one has to take care for avoiding the three-photon absorption. Recent results show that semiconductors, such as ZnTe [11] or GaP [12] can be applied for efficient THz generation, too if longer pump wavelengths are used in order to reduce low order multiphoton absorption. For such long wavelength pumping there is significant refractive index difference between the optical and the THz region in these cases as well. Therefore, the tilted-pulse-front excitation is necessary.

In the tilted-pulse-front excitation geometry the velocity matching reads as [6]

$$v_{p,gr}\cos(\gamma) = v_{THz,ph}\,, \tag{1}$$

where $v_{p,gr}$ is the group velocity of the pump pulse, $v_{THz,ph}$ is the phase velocity of the THz pulse, and γ is the pulse-front-tilt angle. The approximate values of γ are 63° and 69° for LN and LT, respectively, for near infrared pump wavelengths. The highest THz pulse energies in the 0.2 to 1.0 THz range [9] – which is most useful for particle acceleration – are produced in LN based, tilted-pulse-front setups.

In THz generation experiments, perpendicular incoupling of the pump and perpendicular outcoupling of the THz beam are the conditions of minimizing reflection losses and avoiding

Optics EXPRESS

the angular dispersion of the THz beam. Therefore, prism-shaped THz generator crystals with wedge angle equal to the γ pulse-front-tilt are needed. The required large wedge angle negatively affects the THz beam quality for some NMs e. g. LN). This is especially problematic in the case of high energy THz generation experiments, where wide pump beams are needed. The THz wavelets excited at the opposite edges of the pump beam are exposed to different degrees of absorption and dispersion, and the nonlinear effects are also different. Hence the THz wavelets originating from the opposite parts of the pump beam have different intensities and they show different time dependences. Such a bad quality, strongly asymmetric THz beam drastically hinders many applications, especially particle acceleration.

The conventional tilted-pulse-front THz excitation scheme consists of an optical grating, an imaging element and a NM. A so called contact grating scheme was proposed in order to avoid imaging errors [13, 14], which are other important drawbacks of the conventional setup. The optical grating – with a period in the sub-micrometer range – was brought in direct contact with the NM in order to omit imaging. The first suggested contact grating scheme contained a plane-parallel nonlinear crystal [13]. However, it was shown by detailed analysis [15], that optimized, LN based THz generation requires non parallel entrance and exit crystal surfaces, otherwise the necessary oblique outcoupling [16] disadvantageously leads to angular dispersion in the THz beam. The hybrid-type THz pulse source proposed in [10], Tokodi et al. and [17], Pálfalvi et al. is a combination of the conventional and the contact grating setup. In this, the necessary pulse-front-tilt in the nonlinear crystal is created in two steps, namely by diffraction on the conventional grating followed by a demagnification and by diffraction on the contact grating. Since a tilt angle smaller than the final γ is created in the first step, the imaging errors are significantly reduced. The necessary wedge angle is also smaller (~30° for LN, and ~45° for LT) [10, 17] than in the conventional case, but it is still large enough to result in an asymmetric beam.

A modified version of the tilted-pulse-front THz generation was demonstrated by reflecting the pump beam on a stair-step echelon [18] (see Fig. 1). Contrary to the case of the conventional tilted-pulse-front excitation, instead of a continuous pulse-front, a segmented tilted-pulse-front is formed in this case. This kind of pulse-front can be characterized with an average pulse-front-tilt. The tangent of the tilt angle of the average pulse-front – i. e. the (spatial) envelope of the segmented pulse front – in the reflected beam is twice the tangent of the tilt angle of the reflective echelon. The average pulse-front-tilt introduced by the reflection is modified by the imaging element and by the air/NM interface. The γ pulse-front-tilt angle necessary in the NM according to Eq. (1) can be adjusted by the sizes of the stair steps of the reflective echelon – falling in the hundreds of micrometers range – and by the magnification factor of the imaging element. Disadvantageously, this echelon setup also requires a prism-shaped NM with the same γ wedge angle as in the conventional setup.

Optics EXPRESS

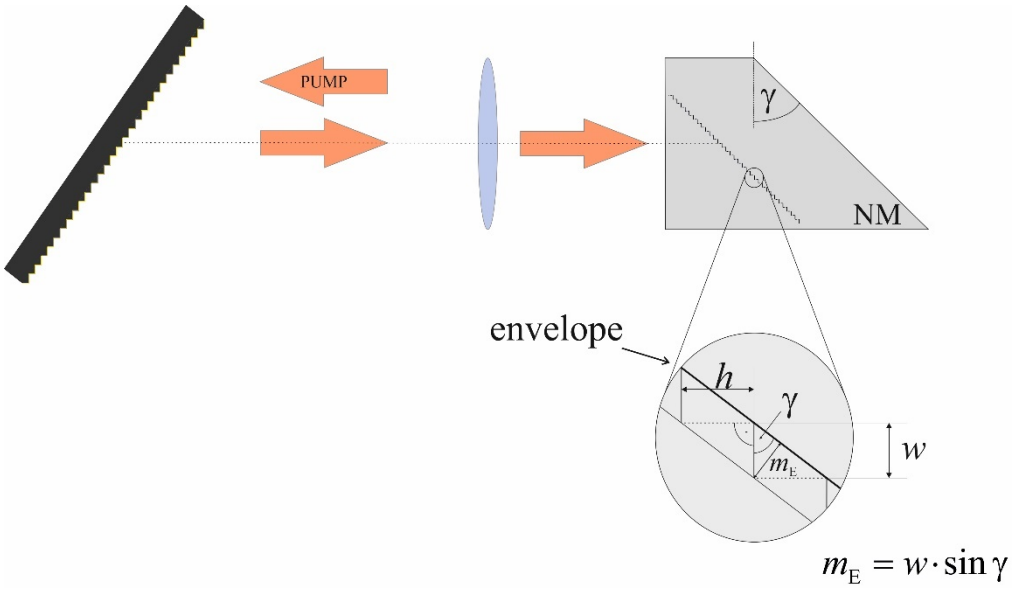

Fig. 1. THz source with a stair-step reflective echelon [18].

In the present paper, we propose and analyze such a hybrid-type setup (see Fig. 2), which is a combination of the conventional scheme, containing diffraction optics and imaging, and a NM with an echelon-like profile created on its entrance surface, hereinafter referred to as "nonlinear echelon slab", NLES. (Let us note here that this NLES based hybrid setup is not to be confused with the earlier proposed hybrid setup [17].) Since the total pulse front tilt is produced in two steps, a beam with reduced angular dispersion falls on the lens, what results in reduced imaging errors. Contrary to all the setups used so far, a plane parallel nonlinear crystal can be used in the NLES based hybrid setup. Hence the absorption, and dispersion are uniform across the output THz beam profile. This advantage, together with the reduced imaging errors, may lead to the realization of a scalable THz pulse source with good output beam quality (i. e. symmetric beam profile) for applications.

We adopted the 1D model originally suggested in [19] and [14] to the NLES based hybrid and the reflective stair-step echelon based setups. Using the corresponding 1D models, the NLES based hybrid, the conventional, and the reflective stair-step echelon based setups are compared based on the numerical results.

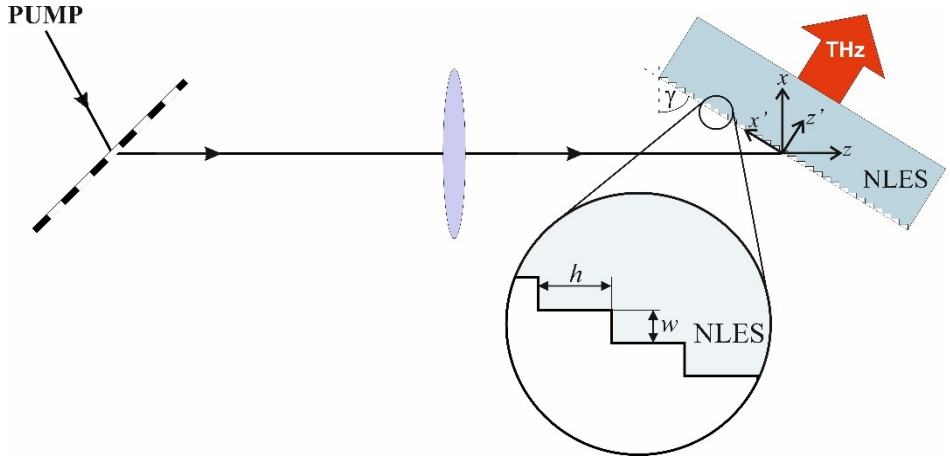

Fig. 2. The scheme of the NLES based hybrid THz source.

Optics EXPRESS

2. Description of the NLES based hybrid setup

The NLES based hybrid setup consists of an optical grating, an imaging element and a NLES as shown in Fig. 2. The echelon slab is made of the material of the nonlinear crystal itself, and has a period in the hundred micrometer range. Its most important advantage compared to all existing and theoretically designed tilted-pulse-front schemes is, that it makes possible the use of a plane-parallel structure if appropriate initial pulse front tilt is applied. This is essential in order to reach good THz beam quality. Furthermore, the NLES based hybrid setup significantly reduces imaging errors compared to the conventional setup and somewhat to the earlier hybrid setup, too.

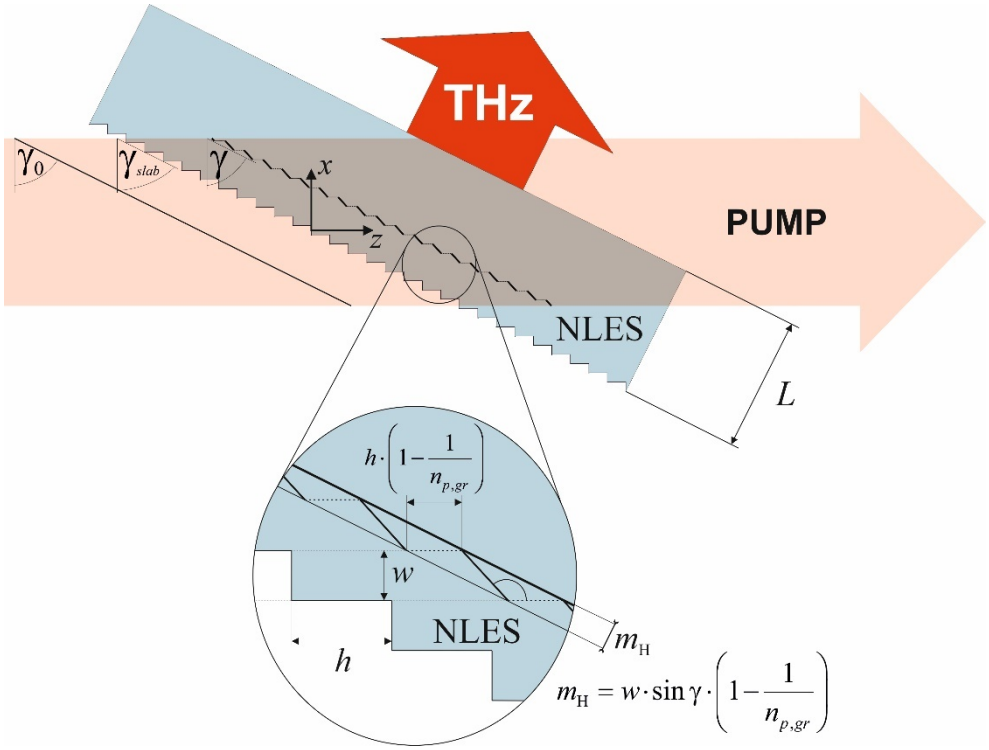

Fig. 3. The alteration of the pump pulse front when passing through the input surface of the NLES.

It is essential to satisfy the velocity-matching condition inside the plane parallel structure, and for the excited THz field it is required to propagate perpendicularly to the output surface. All these imply geometrical conditions. When the pump beam passes through the entrance of the NLES, its pulse-front will be segmented (see Fig. 3). On one hand, the envelope of the NLES entrance (what makes an angle of $\gamma_{slab} = \text{atan}(h/w)$ with the -x direction) has to be parallel to the envelope of the segmented pump-pulse-front inside the NLES (having an average tilt angle of γ). Therefore

$$\gamma = \gamma_{slab} = \text{atan}(h/w) \tag{2}$$

has to be satisfied, where h is the height, w is the width of one echelon step. On the other hand, the condition for the average tilt to remain unchanged while passing through the air/NLES interface is that

$$\gamma_0 = \gamma_{slab} = \gamma \tag{3}$$

Optics EXPRESS

should hold, where γ_0 is the initial pulse-front-tilt of the pump beam directly before reaching the NLES. Please note that the fact that the initial pulse front tilt in front of the entrance of the NLES equals the average pulse front tilt inside the NLES does not mean that the echelon-type entrance has no influence on the pulse front tilt. If the entire input surface would be a plane perpendicular to the propagation direction of the pump beam (as in the conventional setup) the tangent of the tilt angle would be reduced by the ratio of the group refractive indexes when the pump passes through the air/crystal interface. Exactly this happens with any segment of the pulse-front in the present case. However, the $h\cdot\left(1-\frac{1}{n_{p,gr}}\right)$ horizontal shift between the adjacent segments increases the tilt angle of the envelope to the original tilt angle (Fig. 3).

3. Effect of imaging errors

Pump pulse distortions are inherent features of THz source schemes that contain imaging elements. The negative effects of the imaging errors can be mitigated by careful tuning of the systems. An optimization concept concerning the geometry of the conventional setup was given in [14, 20], Fülöp et al. The guideline in those papers is used here for calculating the optimal configuration for the NLES based hybrid setup and for the conventional setup, with the aim of calculating the input pump pulse length along the tilted-pulse-front. This is important, because even in the optimized setups, imaging errors result in pump pulse broadening at the edges of the pump beam resulting in THz beam distortions, which are especially significant when wide beams are used in high energy THz experiments.

For practical reasons, the image plane is set right in front of the NM in the air in both setups, thus $n(\lambda_0)\equiv 1, n_g(\lambda_0)\equiv 1$ in Eq. (13) of [20], obviously. The tilt angle in Eq. (13) of Ref [20]. follows from the phase matching condition, and, in case of LN, has the value of ~77° and ~63° in front of the NM for the conventional setup and for the NLES based hybrid setup, respectively.

Figure 4 shows the local pulse duration at the entrance surface of the nonlinear crystal. LN nonlinear crystal and 200 (a) and 500 fs (b) transformation-limited (TL) pulses with 1030 nm central wavelength were used in the ray tracing calculations. The pump pulse length along the tilted pulse front is plotted versus the *x'* coordinate (*x'* being the axis parallel with the tilted-pulse-front). The top scales show the corresponding *x* coordinate (*x* is the axis in the direction perpendicular to the pump propagation (Fig. 2)).

As shown in Fig. 4, the local pump pulse length increases with the distance measured from the optical axis in all cases. However, in the NLES based hybrid setup, the imaging errors are significantly reduced compared to the conventional setup. Supposing a pump beam diameter of 16 mm and 200 fs pump pulses, the pulse width reduces from 5.6/1.0 ps to 0.75/0.48 ps at the left/right edge of the beam (Fig. 4(a)). The reduction is also very significant for 500 fs pump pulses, where the local pump pulse length reduces from 2200/750 fs to 570/525 fs. As shown in Fig. 4(b), the relative increase of the pump pulse duration remains below 15% along the entire cross-section of the beam in the latter case.

Optics EXPRESS

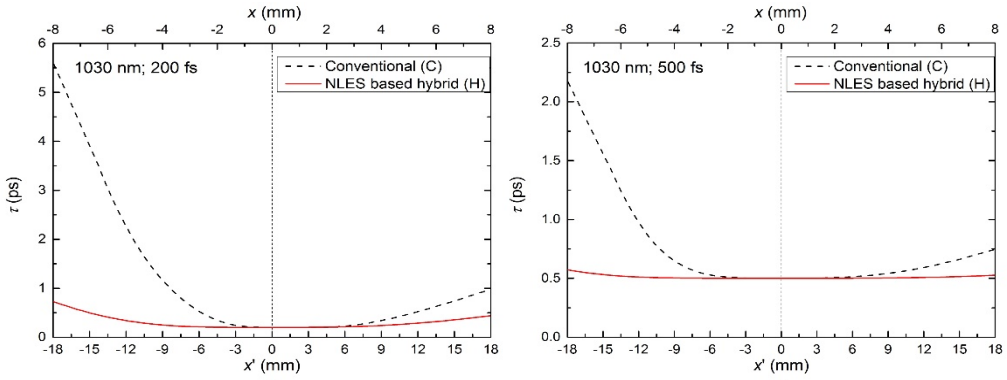

Fig. 4. Pump pulse broadening for 200 (a) and 500 fs (b) TL pulses in the conventional and in the NLES based hybrid setup. The local pump pulse length along the pulse front is plotted versus the *x'* (*x*) coordinate (see text).

In high energy THz generation, where wide pump beams are essential, it is a very important benefit of the NLES based hybrid setup that – due to the lower angular dispersion – the pump pulse remains approximately TL along the entire cross section of the beam. Thus, from this point of view, the NLES based hybrid setup surpasses the conventional THz generation setup. Here we emphasize again, that beside this an even more important advantage of the hybrid-type setup is the possibility of the use of plane-parallel NM.

4. Description of the 1D model

A simple model was developed in order to obtain quantitative information on the optical-to-THz conversion efficiency for three different setups: the conventional, the NLES based hybrid-type and the one proposed by Ofori et al. [18] containing reflective echelon. These setups are denoted by "C", "H" and "E" capitals, respectively hereinafter. The model described in [14], Fülöp et al. and in [19], Vodopyanov for THz generation by optical rectification was adapted to the three different setups by considering some setup-specific effects as well. In the cases of the H and E setups, the transversal variation of the segmented pulse front is taken into account by averaging for one period, hence a one dimensional model is satisfactory.

Let us suppose that the initial waveform of the optical pump pulse is $\tilde{E}(t) = E_0 \exp\left(-2\ln(2)t^2/\tau_0^2\right)\exp\left(i\omega_0 t\right)$, where E_0 is the peak electric field-strength and τ_0 is the TL pump pulse length (FWHM). Taking into account the nonlinear polarization in the same way as in [19], Vodopyanov the differential-equation for the $\mathrm{E}_{THz}\left(\Omega, z'\right)$ Fourier component of the THz field reads as:

$$\frac{\partial}{\partial z'} E_{\mathrm{THz}}(\Omega, z') = -i \frac{\Omega d_{eff} E_0^2 \tau_0}{2\sqrt{4\pi \ln(2)} c n_{THz,ph}(\Omega)} \exp\left(-\frac{\left(\tau_0^2 + \Delta\tau_s\left(z'\right)^2\right)\Omega^2}{16\ln\left(2\right)} \right) \times$$
$$\times \exp\left(i\frac{\Omega}{c}\left(n_{THz,ph}\left(\Omega\right) - \frac{n_{p,gr}}{\cos\left(\gamma\right)} \right) z' \right) f_s\left(z'\right) g_s\left(z'\right) F_s\left(z'\right) - \frac{\alpha_{THz}\left(\Omega\right)}{2} E_{\mathrm{THz}}\left(\Omega, z'\right), \tag{4}$$

where *z'* is the coordinate along the THz propagation direction (Fig. 2), *c* is the speed of light in vacuum, Ω is the angular frequency of the THz radiation, $n_{\mathrm{THz},ph} = c / v_{THz,ph}$ is the THz phase index of refraction, $\alpha_{THz}\left(\Omega\right)$ is the THz (intensity) absorption coefficient, d_{eff} is the

Optics EXPRESS

effective nonlinear coefficient, $n_{p,gr}$ is the group refractive index of the pump. The $\Delta\tau_s(z')$, $f_s(z')$, $g_s(z')$ and $F_s(z')$ are setup-specific functions with s = C, H, E. The meaning and the explanation of these terms are given hereinafter.

$\Delta\tau_s(z')$ is the delay between the short and long wavelength components at the half of the maximum intensity of the pump pulse at z'. Starting from the dispersion parameter, for the case of simultaneous presence of angular and material dispersion [21], one can obtain

$$\Delta\tau_s(z') = \frac{\lambda_0}{c}\frac{z' - a_s\frac{L}{2}}{\cos(\gamma)} n_{p,ph}\left[\left(\frac{b_s}{n_{p,ph}}\lambda_0\tan(\gamma)\right)^2 - \frac{\mathrm{d}^2 n_{p,ph}}{\mathrm{d}\lambda^2}\right]\Delta\lambda, \qquad (5)$$

where λ_0 is the central wavelength of the pump, $\Delta\lambda$ is the spectral bandwidth (FWHM), $n_{p,ph}$ is the phase refractive index at the pump wavelength, L is the length of the NM (Fig. 3). The meaning of a_s and b_s parameters will be clarified below. The role of imaging in the different setups is to reconstruct the TL pump pulse length value along the image plane (which is parallel with the pump pulse front) where the most intensive THz generation is expected [14]. The characteristics of the pump pulse broadening with the propagation (Eq. (5)) is a key factor in the efficiency (Eq. (4)). Good conversion efficiency requires a long spatial region where the pulse length is close to the TL value. If the degree of dispersion is given, a possible way to increase the effective interaction length (defined in [14], Fülöp et al.) is the application of pre-chirped pulses [14, 22]. In this way, one can set the pump pulse length to be minimal (i. e. equal to the TL value) not at the entrance, but inside the crystal, as given by the optimization procedure in [22]. Instead of following this procedure, satisfactory efficiency enhancement can be achieved in a simpler way: by setting the TL pulse length value at the crystal center [14]. Hence, by making the pulse broadening symmetric to the center, the effective interaction length can be nearly doubled, and the efficiency quadrupled. This means that $a_s = 1$ is the proper choice in Eq. (5) if pre-chirped pulses are used, while $a_s = 0$ without pre-chirp.

b_s is also a setup-specific parameter in Eq. (5). It expresses the contribution of the angular dispersion to the pump pulse broadening. Using LN as NM, the effect of the angular dispersion in the pulse broadening is more significant than the effect of the material dispersion [21] in C and H setups. In order to be in agreement with [21], parameter choice of $b_C = n_{p,gr}$ and $b_H = 1$ is required for C and H setups, respectively. Due to the average pulse-front-tilt, angular dispersion is present in the E setup, just as it is in C and H. However, the contribution of the angular dispersion to the pulse lengthening is still negligible for the E setup, since the angular domain is very narrow due to the high (~100) diffraction order. Therefore, the adequate choice is in Eq. (5).$b_E = 0$

The segmented structure of the pump pulse front has an influence on the THz generation in the H and E setups, basically because of three reasons. These are the diffraction of the pump, the periodic phase shift of the THz wavelets, and the discontinuity of the pulse front.

Due to the diffraction of the pump beam, the w' size of one segment of the pulse front varies with the z (and consequently with the z') coordinate (Fig. 5(a)):

Optics EXPRESS

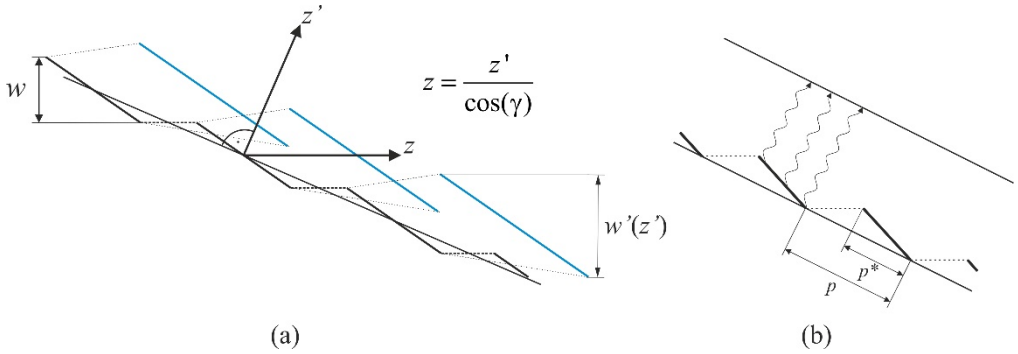

Fig. 5. The influence of the segmented tilted-pulse-front on the THz generation efficiency. The variation of *w'* due to diffraction is shown in (a). (b) illustrates the periodically varying phase-shift, and defines the *p* and *p** parameters.

$$w'(z') = w + \frac{z'\lambda_0}{\cos(\gamma) w n_{p,ph}}. \tag{6}$$

This expansion of the pulse segments results in the decrease of the pump intensity, which is taken into account by a factor of

$$f_s(z') = \frac{w}{w'(z')} = \frac{1}{1 + \dfrac{z'\lambda_0}{\cos(\gamma) w^2 n_{p,ph}}} \tag{7}$$

in Eq. (4) for s = H and E. For the C setup $f_C(z') \equiv 1$, evidently.

The THz wavelets originating from the different points of the segmented pump pulse front experience a periodically varying phase shift due to the differences in the propagation paths to a far plane (see Fig. 5(b)). In order to describe the influence of this effect on the THz generation efficiency, it is useful to introduce the $x_s = m_s / \lambda'$ parameter, which is the ratio of the m_s length (shown in Fig. 1 for s = E, and in Fig. 3 for s = H just behind the crystal entrance) and the THz wavelength inside the crystal ($\lambda' = \lambda_{THz} / n_{\mathrm{THz},ph}$). The factor $g_s(z')$ in Eq. (4) describes the relative decrease of the THz field with respect to the continuous (not segmented) pump pulse front:

$$g_s(z') = \frac{\displaystyle\int_{-x_s\frac{\lambda'}{2}}^{x_s\frac{\lambda'}{2}} E\cos\left(\frac{2\pi z'}{\lambda'}\right) \mathrm{d}z'}{\displaystyle\int_{-x_s\frac{\lambda'}{2}}^{x_s\frac{\lambda'}{2}} E \mathrm{d}z'} = \mathrm{sinc}\left(\pi x_s(z')\right). \tag{8}$$

Taking into account the $w'(z')$ dependence according to Eq. (6), $x_s(z')$ can be given as

$$\begin{aligned} x_H(z') &= m_H(z')\frac{n_{THz,ph}}{\lambda_{THz}} = w'(z')\sin(\gamma)\left(1 - \frac{1}{n_{p,gr}}\right)\frac{n_{THz,ph}}{\lambda_{THz}} = \\ &= \sin(\gamma)\left(w + \frac{z'\lambda_0}{\cos(\gamma) w n_p}\right)\frac{n_{THz,ph}}{\lambda_{THz}}\left(1 - \frac{1}{n_{p,gr}}\right), \end{aligned} \tag{9}$$

Optics EXPRESS

and

$$x_E(z') = m_E(z')\frac{n_{THz,ph}}{\lambda_{THz}} = w'(z')\sin(\gamma)\frac{n_{THz,ph}}{\lambda_{THz}} = \sin(\gamma)\left(w + \frac{z'\lambda_0}{\cos(\gamma)wn_p}\right)\frac{n_{THz,ph}}{\lambda_{THz}} \quad (10)$$

in the H and E setups, respectively. It is important to note that, in this aspect, H is more advantageous than E, since - for the same w value - the corresponding m_s is shortened by a factor of $1-\frac{1}{n_{p,gr}}$, which equals to 0.55 in LN. Evidently, $g_C(z') \equiv 1$ for the C setup.

The $F_s(z') = \mathrm{p}^*/\mathrm{p}$ "duty cycle" (see Fig. 5 (b)) is responsible for the effect of the periodic discontinuity of the pump pulse front observed from the propagation direction of the THz field. Obviously for the C setup $F_C(z') \equiv 1$. $F_s(z')$ can be calculated based on elementary geometry, taking into account the diffraction of the pump beam, too according to Eq. (6):

$$F_H(z') = 1 - \sin(\gamma)\sqrt{\sin^2(\gamma) - \frac{z'\lambda_0}{w^2 n_{p,gr}}}\left(1 - \frac{1}{n_{p,gr}}\right) \quad (11)$$

$$F_E(z') = \cos^2(\gamma)\left(1 + \frac{z'\lambda_0}{w^2 n_{p,gr}\cos(\gamma)}\right) \quad (12)$$

for H and E setups, respectively. For LN NM, the $F_H(0) = 0.57$ obtained value corresponding to the H setup is more advantageous than the $F_E(0) = 0.2$ value corresponding to the E setup.

The effect of absorption (the last term in Eq. (4)) was taken into account in the same manner for the three setups. Only lattice absorption was considered, the effect of multiphoton absorption was neglected. The factor describing the noncollinear velocity-matching (the second exponential factor in Eq. (4)) has also the same form for the three cases. Any other effects, such as imaging errors, cascading effects, and self-phase modulation were neglected.

The THz fluence at the output can be determined from the solution of Eq. (4) as

$$Fluence_{THz} = \frac{c\varepsilon_0}{2} 2\pi \int_0^\infty \left| E_{THz}(\Omega, L)\frac{2n_{THz,ph}}{n_{THz,ph}+1}\right|^2 \mathrm{d}\Omega. \quad (13)$$

The Fresnel reflection, causing a significant loss is also accounted for in this formula. The pump fluence is

$$Fluence_p = \sqrt{\frac{\pi}{2}}\frac{c\varepsilon_0 n_{p,ph}}{2} E_0^2 \frac{\tau_0}{\sqrt{2\ln(2)}}, \quad (14)$$

and the optical-to-THz conversion efficiency is

$$\eta = \frac{Fluence_{THz}}{Fluence_p}. \quad (15)$$

5. Results obtained from the 1D model

Numerical calculations were performed with the model introduced in the previous section in order to have a quantitative picture about the THz generation with the three setups. The supposed NM was stoichiometric LN doped with 0.68 mol% Mg. The temperature was 100 K

Optics EXPRESS

in order to have reduced absorption in the THz range [23]. The absorption coefficient and the refractive index in the THz range were determined experimentally by THz time domain spectroscopy. Optical-to-THz conversion efficiency was calculated as a function of the LN crystal length for a few pump pulse lengths and *w* values.

As it was shown earlier for the C setup, that self-phase modulation and cascading effect lead to strong nonlinear THz beam distortions [24] and they strongly limit the optical-to-THz conversion efficiency [25] in the presence of an intense THz field. These effects are practically negligible below 2% efficiency [25]. Our model, disregarding these effects, is expectedly reliable for the characterization of the different setups, when the efficiency does not exceed 2%.

Detailed comparative analyses have been performed on the H, E and C setups, with special focus on H and E. The efficiencies of E (Figs. 6(a-d)), H (Fig. 6(e-h)) and C (Fig. 6(i)) are depicted versus the crystal length. The TL pump pulse length was supposed to be 100, 200, 500 and 1000 fs in the model calculations. 1030 nm pump wavelength was used, so that three photon absorption would be avoided. The peak pump intensity was kept at a constant value of 40 GW/cm^2 in all cases. For H and C setups, where angular dispersion is significant, pre-chirp of the pump pulse [14] was supposed in order to obtain better efficiencies. $a_H = a_C = 1$ was opted in Eq. (5). Four different step widths, *w* = 40, 60, 80 and 100 μm, were used in the H setup, and *w*-s were chosen in that way in E, that the corresponding m_s values be equal to those in H, for the sake of correct comparison (see Figs. 1 and 3). Therefore, the *w* values in E are smaller by a factor of $1-\frac{1}{n_{p,gr}} = 0.55$, than in H.

Since the efficiency does not exceed the 2% limit in Fig. 6(a-h), there is no doubt about the validity of the predictions of the 1D model in the cases of the E and H setups. The efficiency reaches its maximum within the examined region for both E and H (Fig. 6(a-h)). As it is clearly seen in the figures, the maximum efficiency of the E and H setup increases with increasing *w* at each TL pulse length value, with a single exception for the 100 μm step width in the H setup (Fig. 6(e)). Comparing curves belonging to a given *w* value, the peak efficiency increases with increasing τ_0 in the 100 – 500 fs range for both H and E setups.

As an important result, it was found that the (peak) efficiency values of the H setup are more than ten times larger than those of the E setup. The main reason of this is higher F_s duty cycle (Fig. 5(b)) and higher values of $g(z')$ in H. Comparing the corresponding curves for H and E, it is also obvious, that the efficiency peak is reached at lower *L* crystal length in E. This can be explained by the larger diffraction, that is due to the lower values of the *w* parameter chosen in the E setup.

The spectra, normalized with the same factor, and the corresponding electric field-strengths can be seen in Fig. 7. The curves of 500 fs pump pulse length were chosen, because the efficiencies are reasonably high, and the imaging errors are lower than at shorter pulse lengths. The spectral peaks occur at higher frequencies in the H setup than in E (Figs. 7(a) and (c)). The time dependence of the electric field directly at the output corresponds to quasi single cycle terahertz pulse shape with peak electric field strength of tens of kV/cm (Figs. 7(b) and (d)). These electric field strength values can be increased by at least an order of magnitude by focusing.

Optics EXPRESS

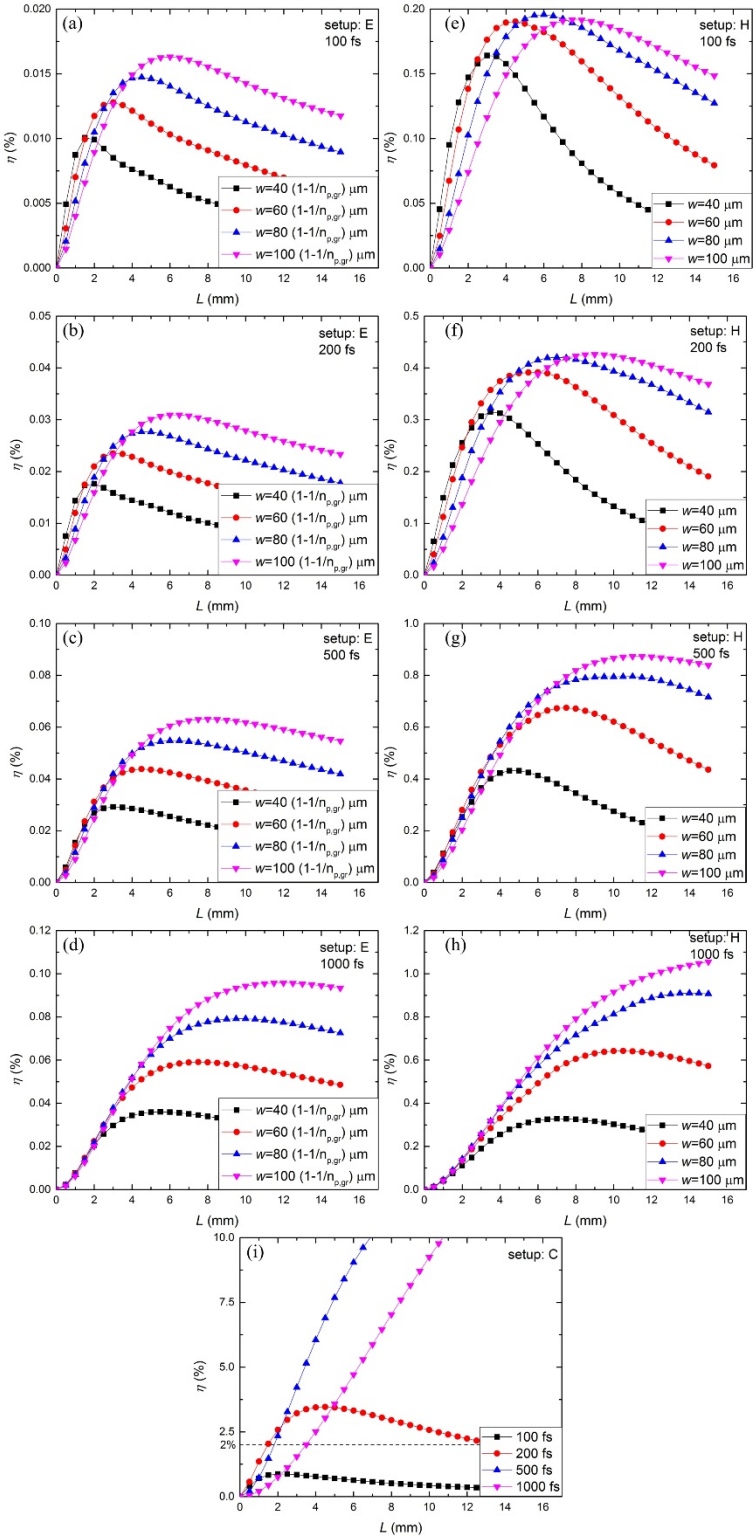

Fig. 6. THz generation efficiency predicted by the model for the H (a-d), E (e-h) and C (i) setups.

Optics EXPRESS

We have to mention here that increased crystal length may lead to the appearance of multi-cycle pulses, because of the overlap between the adjacent segments of the pump pulse front due to diffraction. However, according to simple estimations based on the results shown in Fig. 6, typically, they appear only if the crystal length exceeds its optimal value, and their impact is low due to reduced g_s-factor (Eq. (8)). Therefore, this effect is not relevant in the H setup, especially not in those good-efficiency cases, where w is large (Fig. 6).

While the influence of the specific structure of the segmented pulse front (diffraction, periodic phase shift, discontinuity) reduces the efficiency in the H and E setups, the quickly changing local pump pulse duration (which is the consequence of the large angular dispersion) causes limitation for the crystal length, and for the conversion efficiency in the C setup.

The efficiency of C has also been calculated with the 1D model. The obtained values rapidly increase with τ_0 (Fig. 6(i)). Efficiency values exceeding 2% are not reliable, because of the limiting effects [25] already discussed above, but they are acceptable below 2%.

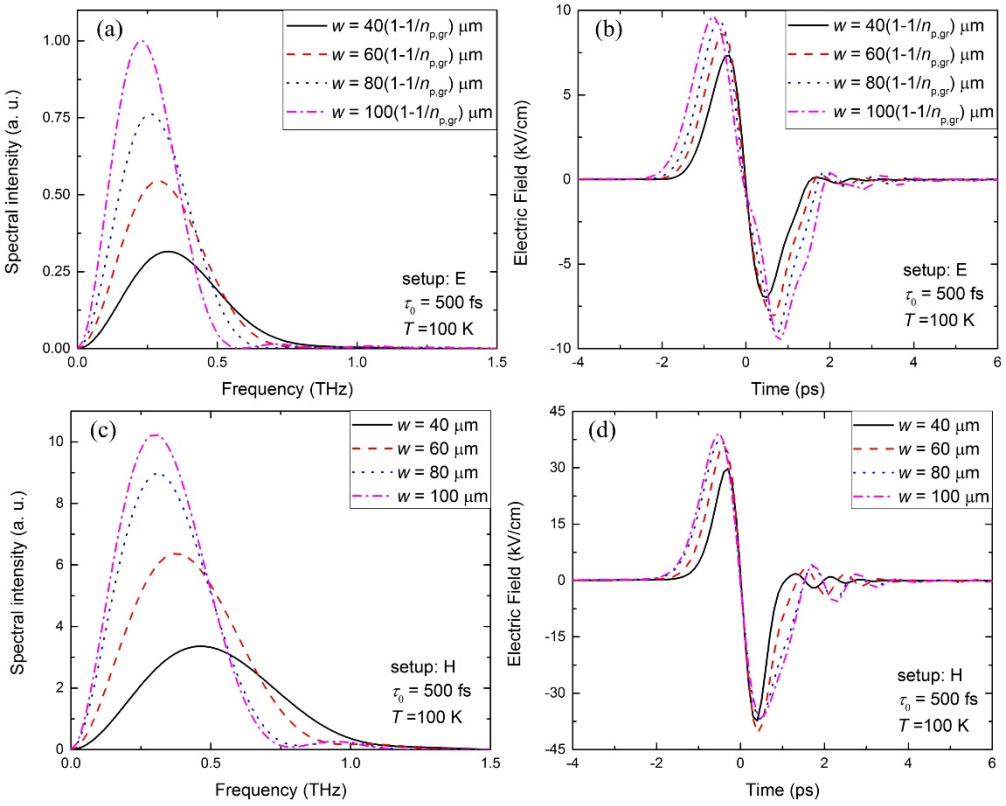

Fig. 7. The spectra and the pulse shapes belonging to the H and E setups for 500 fs pump pulses.

6. Conclusions

A hybrid-type THz source, which is a combination of the conventional tilted-pulse-front setup and a transmission stair-step echelon faced nonlinear crystal with period falling in the hundred micrometer range was proposed for high energy terahertz generation. The suggested short name of this scheme is nonlinear echelon slab (NLES) based hybrid setup. The most important advantage of this setup is the plane parallel structure of the nonlinear crystal, which plays an important role in the efficient production of good quality, symmetric terahertz beam. This advantage manifests itself especially in high energy THz generation experiments, where

Optics EXPRESS

wide pump beams need to be used. Another advantage of the proposed setup is the significant reduction of imaging errors, what is also important in the case of wide pump beams. A 1D model was developed in order to determine the optical-to-terahertz generation efficiency, and was used for quantitative comparison of the NLES based hybrid setup with frequently used arrangements, and especially with an earlier proposed, reflective stair-step echelon containing scheme. The model takes into account the effects coming from the special structure of the pump pulse: the discontinuity, the periodic phase-shift and the diffraction. Calculations applying LN as nonlinear material predict approximately ten times larger efficiency for NLES based hybrid setup than for the reflective stair-step echelon setup. Approximately 1% conversion efficiency and about 0.5 mJ terahertz pulse energy can be reached with the NLES based hybrid setup, when 50 mJ, 500 fs pump pulses with 8 mm beam spot radius are used. The characteristics of the THz pulses predicted by the NLES based hybrid source are especially promising for particle acceleration applications.

Development of a more complex model that considers the cascading effect, self-phase modulation, etc. and the experimental realization of the NLES based hybrid setup are expected in the near future.

Funding

Hungarian Scientific Research Fund (OTKA) (113083); Hungarian Academy of Sciences (MTA) (János Bolyai Research Scholarship); European Union, co-financed by the European Social Fund Comprehensive Development for Implementing Smart Specialization Strategies at the University of Pécs (grant nr. EFOP-3.6.1.-16-2016-00004); the ÚNKP-17-3-I New National Excellence Program of the Ministry of Human Capacities.

Acknowledgment

The present scientific contribution is dedicated to the 650th anniversary of the foundation of the University of Pécs, Hungary.

193.6.62.163 {ts '2018-03-06 11:18:27'}